Corrosion of Al-Sn-Bi Alloys in Alcohol at High Temperatures
Part II: Effect of anodizing on corrosion

Tatsuya Kikuchi[a,*], Yasuhito Hara[a], Masatoshi Sakairi[a], Tetsu Yonezawa[a],
Akira Yamauchi[b], and Hideaki Takahashi[c]
[a]Graduate School of Engineering, Hokkaido University,
N13-W8, Kita-Ku, Sapporo, 060-8628, Japan
[b]Center for Advanced Research of Energy Conversion Materials, Hokkaido University
N13-W8, Kita-Ku, Sapporo, 060-8628, Japan
[c]Asahikawa National College of Technology,
Syunkohdai, 2-2, 1-6, Asahikawa, 071-8142, Japan

*Corresponding author: Tatsuya Kikuchi
TEL: +81-11-706-7112
FAX: +81-11-706-7881

Key words: A. Aluminum alloy; B. SEM; C. Hot corrosion

Abstract

Nine kinds of Al alloys were anodized to form porous anodic oxide films, and then anodized specimens were immersed in 2-(2-(2-methoxyethoxy)ethoxy)ethanol (MEEE) and 2-(2-(2-butoxyethoxy)ethoxy)ethanol (BEEE) at 415 K. Al-1.0%Sn-1.0%Bi alloy was corroded severely in both BEEE and MEEE, whereas other 8 alloys showed no corrosion. The corrosion proceeded under the anodic oxide films through cracks formed in the film. Cathodic polarization in Cu electroplating solution after corrosion suggested that the crack formation during immersion in hot MEEE is due to thermal expansion of the substrate and Sn and Bi containing particles included in the anodic oxide film.

1. INTRODUCTION

Free machining Al alloys containing Sn and Bi are now used in many parts of vehicles and electronic products, and when the alloys are used as the brake cylinder of vehicles, they would be corroded after long exposure to brake-fluids, consisting of high-boiling temperature alcohols. Aluminum and its alloys are known to be corroded in alcohols by the following, alkoxide reaction [1],

$$2Al + 6ROH = 2Al(OR)_3 + 3H_2 \quad (1)$$

In a preceding paper, the authors investigated corrosion of mechanically polished Al alloys in 2-(2-(2-methoxyethoxy)ethoxy)ethanol (MEEE) and 2-(2-(2-butoxyethoxy)ethoxy)ethanol (BEEE) as the main components of brake-fluids [1]. It was found that the addition of Sn or Sn and Bi to pure Al (free machining Al alloys) enhances the corrosion strongly at 415 K, while the addition of Sn or Sn and Bi to Al-Cu and Al-Mg-Si alloys has no effect on the corrosion. The enhancement of corrosion by the addition of Sn or Sn and Bi to pure Al was explained in terms of the enrichment of Sn or Sn and Bi on the specimen surface during immersion, giving rise to galvanic corrosion.

The anodic oxide film formation by anodizing of Al and its alloys generally

improves the corrosion resistance, and the technique may be useful in protecting Al and its alloys from corrosion in hot alcohols. Hatta et al. investigated the corrosion of Al alloys in commercially available brake fluids, which contain MEEE, BEEE, 2-(2-(2-(2-methoxyethoxy)ethoxy)ethoxy)ethanol, and polyalkylene glycol as the main components, and found that anodizing of Al-Sn, and Al-Sn-Bi specimens enhances corrosion to some extent depending on the metallography of specimens [2]. However, it was not clarified why Al alloys with thick anodic oxide films were corroded in hot alcohols.

In this investigation, the effect of anodizing on corrosion of nine kinds of Al alloys, industrially pure aluminum, Al-Cu, and Al-Mg-Si alloys, and Sn or Sn and Bi added to these specimens, in MEEE and BEEE at 415 K was examined. The surface morphology of the anodic oxide films during immersion in MEEE and BEEE was examined by electrochemical measurements and SEM observations, and the corrosion mechanisms of the anodized Al alloys were established.

2. EXPERIMENTAL

2.1 Specimens and pretreatments

Nine kinds of Al alloy disk specimens, 24 mm diameter and 3 mm thick, supplied by Showa Denko K.K., with the chemical compositions of the specimens shown in Table 1. Specimen-10 was industrially pure Al, including small amounts of Fe and Si, and Specimens-13 and -15 were obtained by adding 1.0%-Sn-1.0%-Bi and 1.0%-Sn to Specimen-10. Specimens-10, -13, and -15 were prepared by extrusion and machining. Specimen-20 was an Al-Cu alloy, including 5.0%Cu as well as small amounts of Fe and Si, and Specimens-23, and -25 were obtained by adding 1.0%Sn-1.0%Bi and 1.0%Sn to Specimen-20. Specimens-20, -23, and -25 were prepared by extrusion, heating at 763 K, drawing, aging at 433 K for 24 h, and machining. Specimen-60 was an Al-Mg-Si alloy, including 1.0%Mg and 0.6%Si as well as small amount of Fe. Specimens-63, and -65 were obtained by adding 1.0%Sn-1.0%Bi and 1.0%Sn to Specimen-60. Specimens-60, -63, and -65 were prepared by extrusion, heating at 799 K, ageing at 453 K for 24 h, drawing, and machining. All the specimens were mechanically polished with wet SiC papers of #600, 1000, 1500, and 4000. The mechanically polished specimens were degreased ultrasonically in C_2H_5OH for 10 min, and then kept in a silica gel desiccator prior to anodizing. In addition to Specimens-10 to -65 in Table 1, electropolished highly pure Al plate (99.99 wt%, 2.0 x 2.0 x 0.35 cm^3, Nippon Light Metal Co.) specimens were prepared for comparison of its anodizing behavior with that of the Al alloy specimens.

2.2 Anodizing and pore-sealing

Pretreated specimens were coated with silicone rubber resin at the top half areas so that only the bottom half of specimens were exposed to anodizing solution. Anodizing was carried out for 2 h with a constant current of 100 Am^{-2} in 0.22 M $(COOH)_2$ aqueous solution at 293 K with a Pt counter electrode to form a porous anodic oxide film covering the exposed surface. Time variations in the anode potential, E_a, during anodizing were measured with an Ag/AgCl reference electrode. After anodizing, the specimens were boiled in doubly distilled water for 15 min to seal the pores of the anodic oxide films.

2.3 Immersion tests and rest potential measurements in alcohols

The anodized and pore-sealed specimens were immersed in 20 cm^3 of 2-(2-(2-methoxyethoxy)ethoxy)ethanol (MEEE, molecular weight, M = 164.2 g/mol, boiling point, T_b = 522 K) and 2-(2-(2-butoxyethoxy)ethoxy)ethanol (BEEE, M = 206.3 g/mol, T_b = 551 K) at 415 K for up to t_i = 24 h (t_i: immersion time) with the temperature of the MEEE and BEEE controlled by a silicone oil bath (PS-1000, Tokyo Rikakikai). The mass of the specimens was measured with an ultra microbalance (MX5, METTLER TOLEDO) before (W_1) and after immersion (W_2), and the ratio of the mass change, ΔW (= $W_2 - W_1$) to W_1, was calculated to evaluate the corrosion coefficient, $\Delta W/W_1$. The structural changes in specimen surfaces were examined by digital camera observations, scanning electron microscopy (SEM, Miniscope TM-1000, Hitachi), and electron probe microanalysis (EPMA, JXA-8900M ED/ED, JEOL). For the examination of the vertical cross-sections, specimens were embedded in epoxy resin and polished mechanically to observe a smooth surface cross-section.

Time-variations in the rest potential of the specimens, E vs. t_i (E: rest potential), were measured during immersion in 100 cm^3 of MEEE at 415 K with stirring. The specimens were set in the electrochemical cell with a reference electrode of Pt wire (99.98 wt%, diameter = 0.5 mm, Nilaco). The rest potential of the specimens was measured by a potentiometer (PS-14, Toho Technical Research) during immersion for t_i = 24 h.

2.4 Evaluation of crack formation by Cu decoration method

It was found that cracks were formed in anodic oxide films during immersion of anodized and pore-sealed specimens in BEEE and MEEE, and a Cu decoration method was applied to further elucidate the phenomena. In this method, specimens were first immersed in MEEE for 24 h at 293 K and then cathodically polarized in 0.63 M $CuSO_4$ / 0.50 M H_2SO_4 solution at a constant potential of E_c = -0.25 V (vs. Ag/AgCl) to measure the current transient during cathodic polarization. The copper deposition due to the cathodic polarization was observed by SEM.

3. Results

3.1 Structure and formation of anodic oxide films

Fig. 1 shows the time-variations in the anode potential during anodizing of alloy specimens and the highly pure Al specimen at 100 A m^{-2} in 0.22 M $(COOH)_2$ at 293 K. The highly pure Al specimen (4N-Al) shows an even potential of around 50 V after a short transient period. The anode potentials of Specimens-10, -13, and -15 rise slightly with anodizing time after an initial rapid rise, and the value of the potentials at the second stage is in the order of Specimen-10, -15, -13 and 4N-Al. The anode potentials of Specimens-20, -23, and -25 become almost steady at about 3600 s, and the steady value of Specimen-20 is much higher than that of the highly pure 4N-Al, while the steady values of Specimens-23 and -25 are lower. Gas evolution was observed on these specimens during anodizing, and Cu was deposited on the Pt counter electrode as a result of dissolution of copper from the substrate alloys. The anode potentials of Specimens-60, -63, and -65 reach steady values relatively early, and the steady values of these three specimens are higher than that of the highly pure Al. Gas evolution was also

observed on these specimens during anodizing, and the gas evolution rate on these specimens was lower than that on Specimens-20, -23, and -25. It is clear from Fig. 1 that the potential-variation during anodizing strongly depends on the metallography of the specimens, and that the addition of Sn or Sn and Bi to Specimens-10 and -20 lowers the anode potentials, while no such clear change is observed by the addition of Sn or Sn and Bi to Al-Mg-Si alloy.

Fig. 2 shows SEM images of vertical cross-sections of (a) Specimens-10, (b) -13, and (c) -15, respectively, after anodizing for 2 h with a constant current of 100 A m^{-2} in 0.22 M $(COOH)_2$ at 293 K. All the images show three layers consisting of resin (top layer), anodic oxide film (middle layer), and the substrate (bottom layer). White thin layer between resin and oxide is an artifact due to strong electron reflection by narrow channels. All the specimens are covered with uniform anodic oxide films, with thicknesses of 30, 20, and 30 μm respectively on Specimens-10, -13, and -15. The EPMA identified the white small areas in Specimen-13 as Sn and Bi. Al and Bi are entirely immiscible in the liquid state. The solid solubility of Sn in Al is low and that of Bi in Sn is not high. Thus, Sn and Bi seemed to be formed by eutectic solidification after monotectic solidification of the α−Al phase, and Sn and Bi in the particles of a few μm in diameter could not be identified separately by EPMA. Hereafter, they will be called Sn-Bi particles. The Sn-Bi particles are present in the anodic oxide film as well as in the substrate. This suggests that Sn-Bi particles included in the substrate are taken up into anodic oxide films during the film growth. The Sn particles included in the substrate of Specimen-15 may be taken up into the anodic oxide film during anodizing (see Fig. 2(c)).

Fig. 3 shows SEM images of vertical cross-sections of: (a) Specimens-20, (b) -23, (c) -25, (d) -60, (e) -63, and (f) -65 after anodizing for 2 h at a constant current density of 100 A m^{-2} in 0.22 M $(COOH)_2$ at 293 K. The anodic oxide films formed on Specimens-20, -23, and -25 are relatively thin, 17, 10, and 15 μm, and have numerous void-type imperfections (Fig. 3(a), (b), and (c)). This is due to preferential dissolution of the Al_2Cu phase and O_2 gas evolution during anodizing [1, 3]. The anodic oxide films formed on Specimens-60, -63, and -65 are relatively thick, 30, 28, and 30 μm, and have fewer imperfections than the films on Specimens-20, 23, and 25. The EPMA measurements showed that the anodic oxide films formed on Specimens-63 and -65 include Sn-Bi particles and Sn particles but no Mg.

3.2 Corrosion behavior in MEEE and BEEE at 415 K up to 24 h

Fig. 4 shows the appearance of anodized specimens after immersion for 24 h in MEEE at 415 K. The top half of the specimens was covered with silicone resin and the bottom half was exposed to the MEEE. The anodic oxide films formed in oxalic acid solution showed a yellowish color and the color of all the specimens except Specimen-13 was practically unchanged after the immersion in MEEE at 415 K for 24 h. Immersion in MEEE resulted in some striped patterning of the specimens. Specimen-13 shows a grey surface. A significant thinning of the specimen was also found as a result of severe corrosion. In immersion in BEEE at 415 K for 24 h (Fig. 5), the corrosion effects are similar to those in MEEE, showing severe corrosion of only Specimen-13. The photograph of Specimen-13 indicates that silicone resin has been removed during the immersion. A corrosion pattern can be seen due to cracking of anodic oxide film on

the bottom half of the specimen. The mass changes of Specimen-13 immersed in MEEE and BEEE at 415 K for 24 h were $\Delta W/W_1$ = - 29.2 % and -14.6 %, respectively, while other specimens showed only -0.5 % < $\Delta W/W_1$ < 0.5 % mass changes.

Fig. 6 shows the time-variations in the rest potential, E, of Specimens-10, -13, and -15 during immersion in MEEE at 415 K. The rest potential of Specimen-10 rises quickly at the initial stage and then reaches a steady value of about 0 V (vs. Pt). The rest potential of Specimen-15 fluctuates between -0.3 V and -0.5 V. For Specimen-13, the rest potential drops at the initial stage, reaches a minimum, and then rises to reach a steady value of -1.2 V at 8 h of immersion time.

Fig. 7 shows the appearance of Specimen-13 after immersion for 2.5 h at 415 K in (a) MEEE and (b) BEEE. In both cases, Specimen-13 shows a corrosion pattern due to cracking of anodic oxide film and the corrosion in MEEE is more complicated and extensive than in BEEE. The corrosion based on cracking of the anodic oxide film is shown in more detail in the SEM images in Fig. 8. Figs. 8(a) (low magnification) and (b) (high magnification) are SEM images of the surface of Specimen-13 after immersion in MEEE for 4 h at 415 K. The images show color-changed areas along the cracks. More details of the color-changed areas can be seen in the SEM image of a vertical cross-section of the specimen (Fig. 8(c)). The crack is only 1 μm wide and the corroded area under the crack spreads widely, the width of which is larger than 100 μm. The color-changed areas in Figs. 8(a) and (b) correspond to the corroded areas underneath the crack. It must be noted here that the surface of the corroded area is uneven and that Sn and Bi are enriched at the surface. A similar corrosion process can be expected in BEEE on anodized/pore-sealed Specimen-13, although SEM observation of the vertical cross section was not carried out.

3.3 Crack formation revealed by Cu decoration method

Fig. 9 shows the time-variations in the cathodic current during cathodic polarization at -0.25 V (vs. Ag/AgCl) in 0.63 M $CuSO_4$ / 0.50 M H_2SO_4 at 293 K, measured after Specimen 13 was immersed for 2 h and other specimens for 24 h in MEEE at 415 K. It can be seen from Fig. 9(a) that the cathodic current, i_c, increases with polarization time, t_c, on Specimen-13, while no current is observed on Specimens-10 and -15. On Specimens-23 and -25, i_c increases with t_c but there is no current flow on Specimen-20 (b). The values of i_c at t_c = 15 min on Specimens-23 and -25 are much larger than the value on Specimen-13. The i_c on Specimen-63 shows an increase with t_c, and no current flows on Specimen-60. The i_c on Specimen-65 shows a very slight increase after t_c = 15 min.

Fig. 10 shows SEM images: (a, b) Specimens-13, (c, d) -23, and (e, f) -25 after cathodic polarization for 10 min at -0.25 V (vs. Ag/ AgCl) in 0.63 M $CuSO_4$ / 0.50 M H_2SO_4 at 293 K. The images in Figs. 10(a), (c), and (e) are low magnification, and those shown in Figs. 10(b), (d), and (f) are high magnification. The specimens were immersed in MEEE at 415 K for 2 h (Specimen-13) or 24 h (Specimens-23 and -25) before the cathodic polarization. There are white granular deposits in a linear line-up on Specimen-13 (Fig. 10(a)), and these grains are copper particles deposited on the anodic oxide films by the cathodic polarization in $CuSO_4$ solution (Fig. 10(b)).

$$Cu^{2+} + 2e^- = Cu \qquad (2)$$

This fact found for Specimen 13 clearly indicates that copper deposition occurs at the

cracks in the anodic oxide films due to exclusive passage of deposition current through the cracks. The whole surface of Specimen-23 is covered with Cu deposited. This reveals the extensive development of cracks in the anodic oxide films on Specimen-23 during immersion in the hot MEEE (Figs. 10(c) and (d)). Copper particles are also deposited on Specimen-25 through cracks (Figs. 10(e) and (f)).

Fig. 11 shows SEM images of (a, b) Specimen-63, and (c, d) Specimen-65 after cathodic polarization for 10 min. The conditions of immersion in MEEE (24 h, 415 K) and the cathodic polarization are the same as those in Fig. 10. On both Specimens-63 and -65, Cu particles are deposited on the surface, and the number of Cu particles is much larger on Specimen-63 than on Specimen-65. The SEM images of Specimens-10, -15, -20, and -60 did not show evidence of the deposition of Cu on the surface.

Comparison of Fig. 9 with Figs. 10 and 11 indicates that the Cu decoration method assists the elucidation of the formation of cracks in the anodic oxide films during immersion in MEEE. Cracks formed on Specimens-13, -23, -25, -63, and -65 during the immersion in MEEE at 415 K, while no cracks formed on Specimens-10, -15, -20, and -60, and the extent of cracking of the anodic oxide films during immersion in MEEE decreases in the order of Specimens-23 > -63 > -25 >> -13 > -65.

To further check details of the mechanism of the crack formation in the anodic oxide film on Specimen-13 in MEEE, the specimen was heated in air at 415 K for 2 h. The SEM observations (images not shown) of the heated specimen showed the crack formation. This strongly suggests that thermal expansion of the substrate metal and Sn-Bi particles in the oxide during immersion in the hot MEEE is responsible for the formation of cracks in the anodic oxide films.

4. Discussion

4.1 Mechanisms of corrosion of anodized specimens in MEEE and BEEE

As described in 3.2, only Specimen-13, covered with anodic oxide films, is corroded severely in MEEE and BEEE at 415 K for 24 h. In a preceding investigation [1], immersion tests of mechanically polished specimens were carried out under the same conditions as here, and it was found that Specimens-13 and -15 were corroded severely in MEEE and only Specimen-15 was corroded in BEEE. Therefore, it is clear that the anodizing/pore-sealing protects Specimen-15 from corrosion in both alcohols due to the isolation of the substrate by the anodic oxide film because the anodic oxide film on Speciemen-15 without containing Bi was not cracked by the thermal shock induced by immersion in the hot alcohols.

On the contrary, the anodizing/pore-sealing resulted in corrosion of Specimen-13 in both alcohols. This fact can be explained as follows. The anodized Specimen-13 is covered with porous anodic oxide film that contains numerous Sn-Bi particles, as shown in Fig. 2(b). Immersion of the anodized specimen in boiling water causes hydroxide to form in the pores, leading to pore-sealing. The oxide film becomes more brittle by the pore-sealing. When the anodized/pore-sealed Specimen-13 is immersed in MEEE and BEEE at 415 K, it expands thermally. Hence, tensile stress may develop in the oxide film laterally, since the thermal expansion coefficient of Al is about three-times as high as that of Al_2O_3. The Sn-Bi particles included in the oxide film may exacerbate the tensile stress by their thermal expansion (Fig. 12(a)). Hence, cracks are formed in the oxide films, and these allow MEEE and BEEE to penetrate to reach the

interface between the anodic oxide film and the substrate (Fig. 12(b)). At the interface beneath the cracks, there are the α–Al phase and Sn-Bi particles exposed to BEEE and MEEE, and corrosion occurs by the following equations.

$$2Al + 6ROH = 2Al(OR)_3 + 6H^+ + 6e^- \quad (3)$$

$$6H^+ + 6e^- = 3H_2 \quad (4)$$

Evolution of H_2 gas occurs on the Sn-Bi particles exposed to BEEE and MEEE (Fig. 12(c)), and the Sn-Bi particles act as a local cathode in the galvanic corrosion. In the progress of corrosion, Sn-Bi particles accumulate on the surface of the substrate, leading to an acceleration of corrosion with time. Eventually, a sponge-like layer of Sn-Bi covers the whole surface [1].

The time-variations in the rest potential of Specimen-13 in MEEE (see Fig. 6) can be explained as follows. The drop of the rest potential with t at the initial stage of immersion before t = 4 h is due to the exposure of the substrate to MEEE through the cracks, and the rise in the rest potential between t = 4 – 8 h of immersion may be explained by enrichment of Sn-Bi particles on the surface of the substrate corroded beneath the cracks. The steady rest potential at -1.2 V after t = 8 h of immersion may correspond to the rapid corrosion with a sponge-like Sn-Bi layer at the surface of the substrate as reported in [1]. Incidentally, the steady rest potential of Specimen-10 at about 0V corresponds to the corrosion inhibition by stable pore-sealed anodic oxide films, and the relatively large fluctuation in E between -0.5 and -0.3 V with Specimen-15 during immersion corresponds to the repeated cycles of repair and development of imperfections in the anodic oxide film.

It must be noted, here, that the anodized/pore-sealed Specimen-13 is corroded by immersion in BEEE at 415 K for 24 h (Fig. 5), although the mechanically polished specimen was not corroded under the same immersion conditions [1]. This is a phenomenon opposite to that for Specimen-15: corrosion after mechanical polishing versus absence of corrosion after anodizing/pore-sealing. The potential change of Specimen-15 can be simply explained by the corrosion inhibition of the anodic oxide films, but the potential change of Specimen-13 cannot be accounted for in this manner. However, it may be due to the relatively less aggressive properties of BEEE and the absence of crack formation in a thin flexible oxide film formed during mechanical polishing.

4.2 Effect of the film structure on the crack formation

Anodic oxide films formed on the nine specimens in this investigation have the following structural characteristics.

1) The film thickness decreases in the order of Specimen-10, -15, -60, -65 > -63 > -13 > -20, -25 > -23. In other words, the Al-Cu alloys have relatively thinner oxide films, and the alloying of pure Al, Al-Cu, and Al-Mg-Si alloys with Sn or Sn and Bi causes the thickness of anodic oxide films to decrease. This is due to the low current efficiency of film formation during anodizing arising from the preferential dissolution of the Al_2Cu phase and O_2 gas evolution [4].

2) Among alloying elements, Cu and Mg dissolve into the anodizing solution during anodizing [5], while Si, Sn, and Sn-Bi particles are taken up into the anodic oxide films rather than dissolved. Hence, anodic oxide films formed on Al-Cu alloys incorporate numerous void-like imperfections, and the oxide films formed on Sn- and Sn-Bi-alloyed specimens include a great number of Sn- and Sn-Bi particles.

As described in 3.3, no cracks are formed in the anodic oxide films on Specimens-10, 15, 20, and 60 by the immersion in MEEE at 415 K for 24 h, and the development of cracks in anodic oxide films is less pronounced in the order of Specimens-23 > -63 > -25 >> -13 > -65. This suggests that the crack formation is more closely related to the amount of Sn and Sn-Bi particles in the anodic oxide films rather than the film thickness. S. Rossi et al. investigated the corrosion of anodized Al-Bi alloys in aqueous solutions, and found that Bi-inclusions embedded in anodic oxide films are a cause of the crack formation, leading to local corrosion under the film [6].

The absence of corrosion of the anodized/pore-sealed Specimens-10, -15, -20, and -60 in MEEE and BEEE at 415 K for 24 h can be simply understood to be due to the isolation of the substrate with a stable anodic oxide film. However, no corrosion of Specimens-23, -25, -63, and -65 after the anodizing/pore-sealing cannot be explained by the isolation with the anodic oxide film, since cracks are formed during immersion. Specimens-23, -25, -63, and -65 after mechanical polishing were not corroded in MEEE and BEEE in the first report [1], and this was explained by a lower galvanic action of Sn or Sn and Bi phases possibly due to the formation of compounds such as Sn_2Cu and Sn_7Mg_3 [7]. The behavior of the specimens covered with anodic oxide films may also be explained by a similar action to that on the mechanically polished specimens. During immersion cracks are formed in the anodic oxide film to expose a fresh surface of the substrate to MEEE and BEEE, but an appreciable galvanic corrosion did not occur due to the lower catalytic activity of the exposed compounds.

In summary, it must be noted that anodizing and pore-sealing of free machining Al alloys inhibited corrosion of Al-Sn alloys in the presence of the components of brake fluid (MEEE and BEEE) at high temperatures, but that Al-Sn-Bi alloy is corroded in this environment by the formation of cracks in the anodic oxide films. The findings here stress the need for care when using or specifying Al-Sn-Bi alloys covered with anodic oxide film in brake cylinders of vehicles due to the potential for severe corrosion.

5. Conclusions

In this investigation, nine kinds of Al alloys, with and without addition of Sn or Sn and Bi, were examined to clarify the effects of anodizing and pore-sealing on the corrosion of the alloys in MEEE and BEEE at 415 K for 24 h, and the following conclusions may be drawn.

1) Anodized and pore-sealed Al-1.0%Sn-1.0%Bi alloy is corroded severely in both MEEE and BEEE, and the corrosion proceeds under the anodic oxide films through cracks formed in the film. In the process of corrosion, Sn-Bi particles accumulate on the corroded surface and act as local cathodes to accelerate the corrosion.
2) The crack formation is due to the lateral tensile stresses imposed on the oxide film by thermal expansion of the substrate and the Sn-Bi particles included in the oxide film.
3) The Al, Al-Sn, Al-Cu, and Al-Mg-Si alloys without addition of further alloying elements are not corroded by MEEE and BEEE due to the isolation of the substrate by the covering stable anodic oxide films. No corrosion of Al-Cu-Sn, Al-Cu-Sn-Bi, Al-Mg-Si-Sn, and Al-Mg-Si-Sn-Bi alloys is due to a weakening in the cathodic action of the second phases by the formation of metallic compounds like Sn_2Cu and Sn_7Mg_3.

Acknowledgements

This work was financially supported by the Japan Aluminum Association. The authors express their appreciation to the members of the Working Group for Tin-containing Aluminum Alloys, for their preceding work and for helpful discussion. The authors also thank Mr. Kazuhiko Minami (Showa Denko) and Dr. Ken Ebihara (Nippon Light Metal) for supplying the Al specimens.

References

[1] T. Kikuchi, Y. Hara, M. Sakairi, T. Yonezawa, A. Yamauchi, and H. Takahashi, Corr. Sci., 52 (2010) 1482-1491.

[2] H. Hatta, Y. Shoji, Y. Kato, S. Yoshiwara, R. Shoji, K. Mori, I Iwai, and K. Minami, Abstract of 113th Biannual Meeting of Jpn. Inst. of Light Metals (2007) 201-202.

[3] H. Takahashi, K. Watanabe, R. Furuichi, and M. Seo, Proc. of 7th Asian Pacific Corros. Control Conf. 2 (1991) 995-1000.

[4] H. Takahashi, K. Shiga, K. Watanabe, and M. Seo, J. Surf. Fin. Soc. Jpn. 44 (1993) 542-548.

[5] S. Z. Chu, M. Sakairi, H. Takahashi, K. Shimizu, and Y. Abe, J. Electrochem. Soc. 147 (2000) 2182-2189.

[6] S. Rossi, F. Deflorian, and L. Maines, Benelux Metallugie 45 (2006) 299-305.

[7] T. Lyman, Metals Handbook: Metallography, Structures and Phase Diagrams, eighth ed., American Science of Metals, Metals Park, OH, USA, 1973.

Captions

Table 1 Chemical compositions of the Al alloys (mass%) in this investigation.

Fig.1 Changes in the anode potential, E_a, during anodizing in 0.22 M $(COOH)_2$ solution at 293 K and 100 A/m^2 on: (a) Specimens-10, -13, -15, 4N-Al; (b) -20, -23, -25, 4N-Al; (c) -60, -63, -65, and 4N-Al.

Fig. 2 SEM images of vertical cross-sections of (a) Specimens-10, (b) -13, and (c) -15 after anodizing for 2 h.

Fig. 3 SEM images of vertical cross-sections of (a) Specimens-20, (b) -23, (c) -25, (d) -60, (e) -63, and (f) -65 after anodizing for 2h.

Fig. 4 Surface appearance of anodized specimens after immersion in MEEE at 415 K for 24 h.

Fig. 5 Surface appearance of anodized specimens after immersion in BEEE at 415 K for 24 h.

Fig. 6 Changes in rest potential, E, with immersion time, t_i, in MEEE at 415 K of anodized Specimens-10, -13, and -15.

Fig. 7 Surface appearance of Specimen-13 immersed for 2.5 h at 415 K: (a) MEEE and (b) BEEE.

Fig. 8 SEM images of the surface and a vertical cross-section of Specimen-13 immersed in MEEE at 415 K for 4 h: (a) surface at low magnification, (b) surface at high magnification, and c) vertical cross-section.

Fig. 9 Time-variations in the cathodic current, i_c, during cathodic polarization at -0.25 V (vs. Ag/AgCl) in 0.63 M $CuSO_4$ / 0.50 M H_2SO_4 at 293 K, obtained for: (a) Speciemens-10, 13, -15; (b) -20, -23, -25; (c) -60, -63, and -65, all after immersion in MEEE at 415 K.

Fig. 10 SEM images of (a, b) Specimens-13, (c, d) -23, and (e, f) -25 after cathodic polarization for 10 min at -0.25 V (vs. Ag/AgCl) in 0.63 M $CuSO_4$ / 0.50 M H_2SO_4 at 293 K. The left images (a, c, e) are low and the right images (b, d, f) are high magnifications. All the specimens were immersed in MEEE at 415 K before the cathodic polarization.

Fig. 11 SEM images of (a, b) Specimens-63 and (c, d) -65 after cathodic polarization for 10 min at -0.25 V (vs. Ag/ AgCl) in 0.63 M $CuSO_4$ / 0.50 M H_2SO_4 at 293 K. The left images (a, c) are low and the right images (b, d) are high magnifications. All the specimens were immersed in MEEE at 415 K before the cathodic polarization.

Fig. 12 Schematic illustration of the corrosion of the anodized and pore-sealed Specimen-13 in MEEE (a) crack formation, (b) MEEE penetration to the interface between anodic oxide film and the substrate, and (c) corrosion of the substrate by the accumulation of Sn-Bi particles on the corroding surface of the specimen.

Table 1

No.	Sn	Bi	Cu	Mg	Si	Fe	Al
10	-	-	-	-	0.1	0.3	bal.
13	1.0	1.0	-	-	0.1	0.3	bal.
15	1.0	-	-	-	0.1	0.3	bal.
20	-	-	5.0	-	0.2	0.3	bal.
23	1.0	1.0	5.0	-	0.2	0.3	bal.
25	1.0	-	5.0	-	0.2	0.3	bal.
60	-	-	0.3	1.0	0.6	0.3	bal.
63	1.0	1.0	0.3	1.0	0.6	0.3	bal.
65	1.0	-	0.3	1.0	0.6	0.3	bal.

(a) Specimen-10, -13, and -15

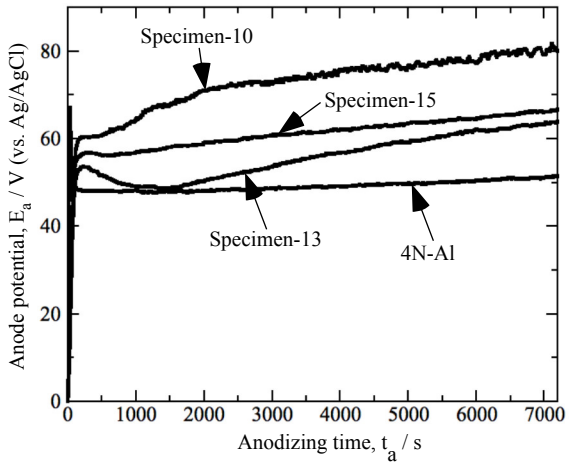

(b) Specimen-20, -23, and -25

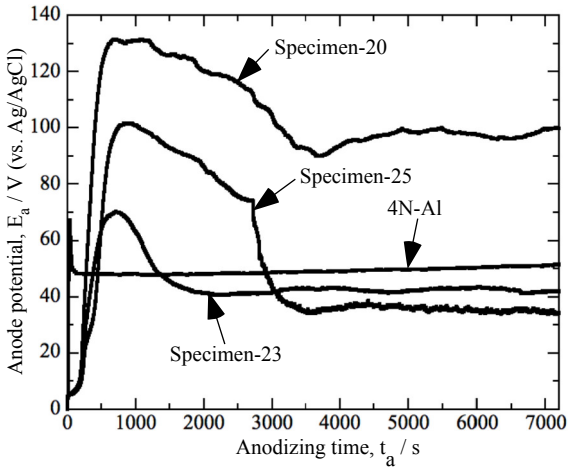

(c) Specimen-60, -63, and -65

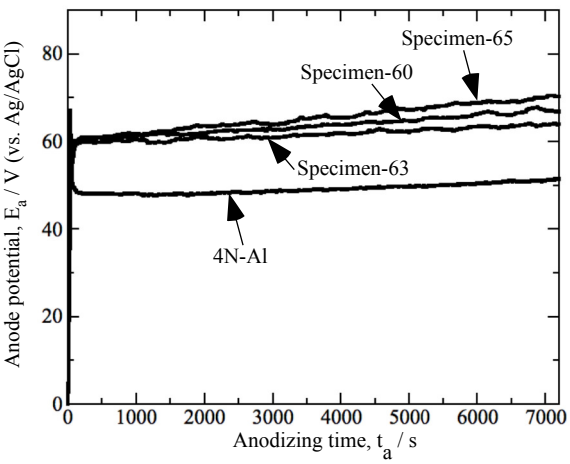

Fig. 1

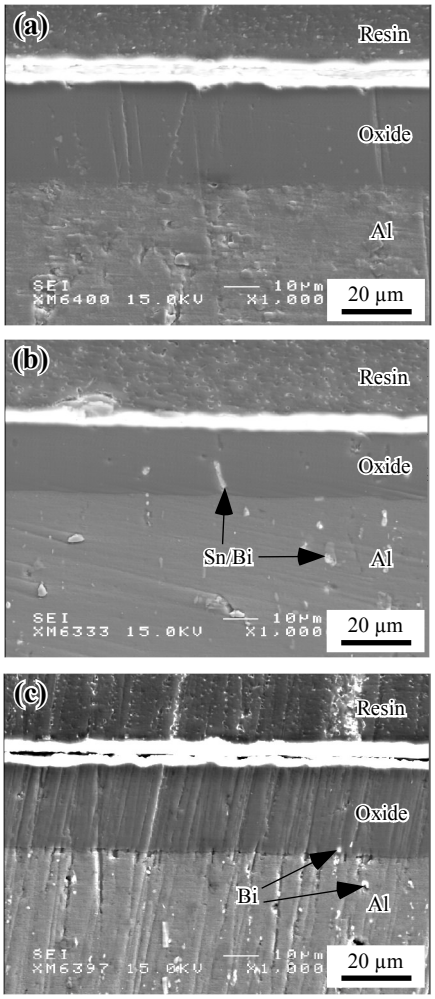
(a)
Resin
Oxide
Al
SEI
XM6400 15.0KV
10μm
X1,000
20 μm
(b)
Resin
Oxide
Sn/Bi
Al
SEI
XM6333 15.0KV
10μm
X1,000
20 μm
(c)
Resin
Oxide
Bi
Al
SEI
XM6397 15.0KV
10μm
X1,000
20 μm

Fig. 2

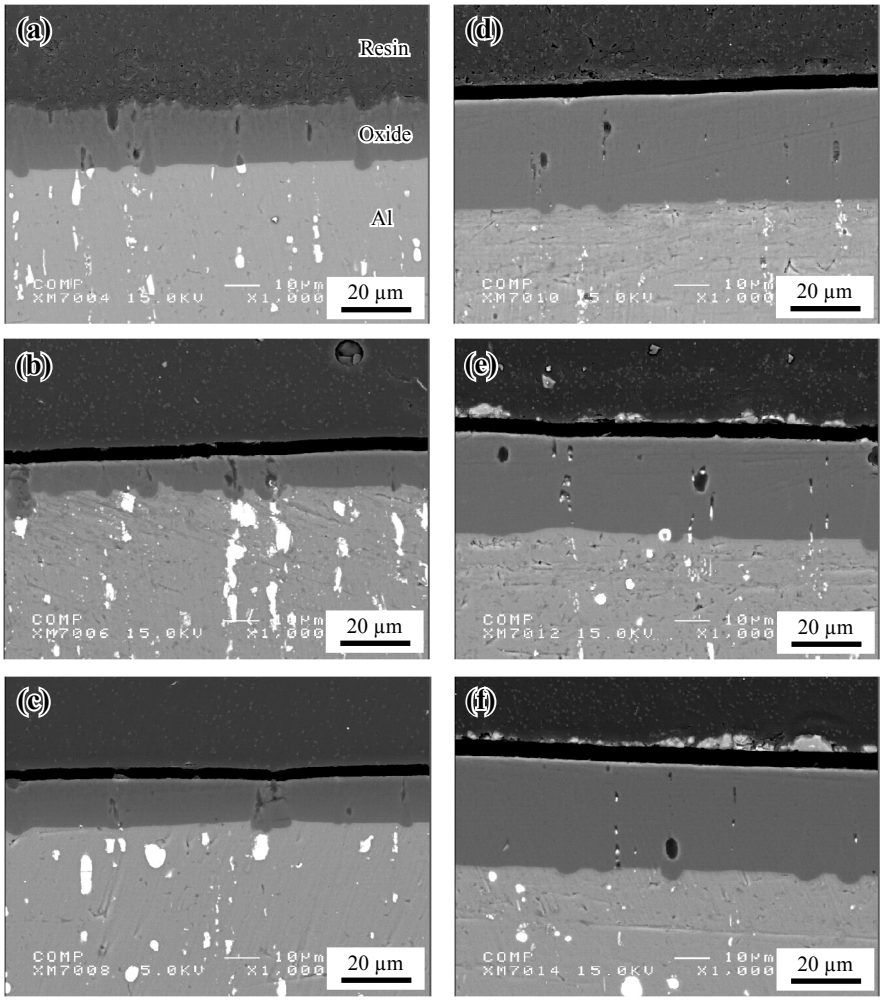

Fig. 3

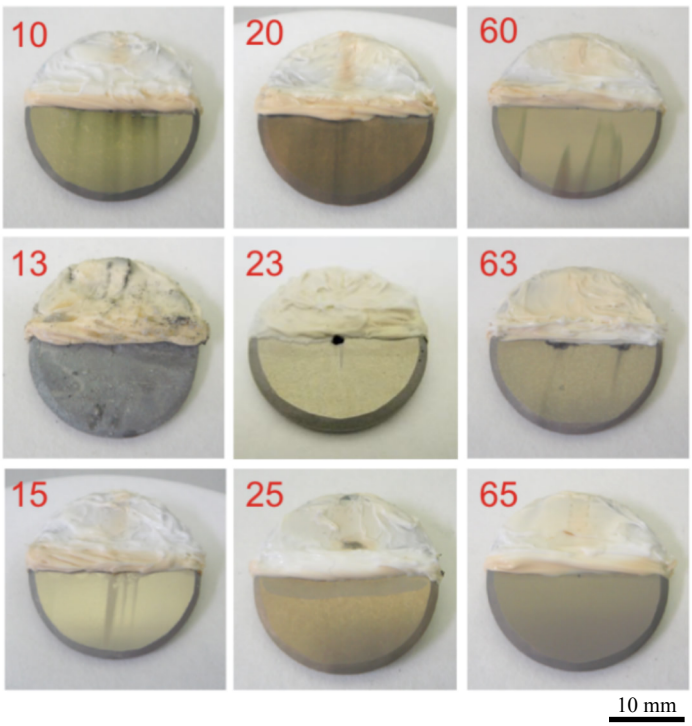

Fig. 4

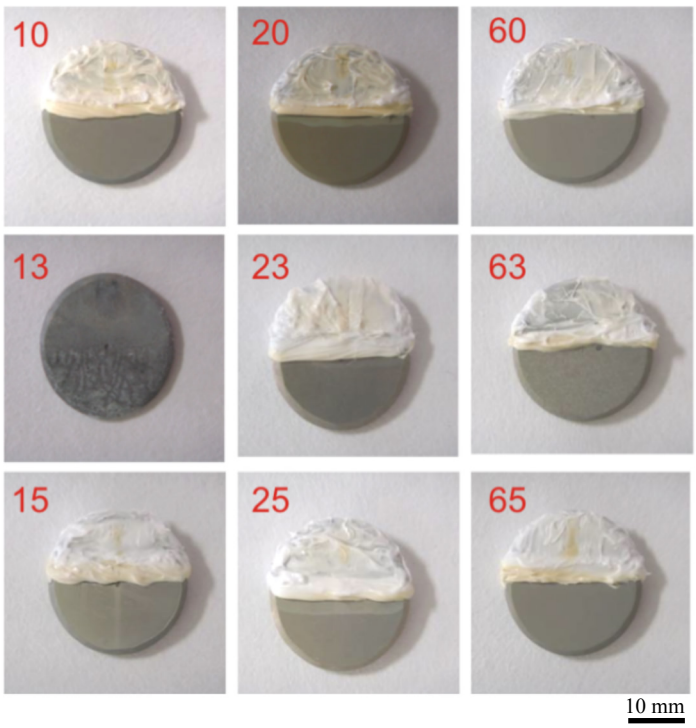

Fig. 5

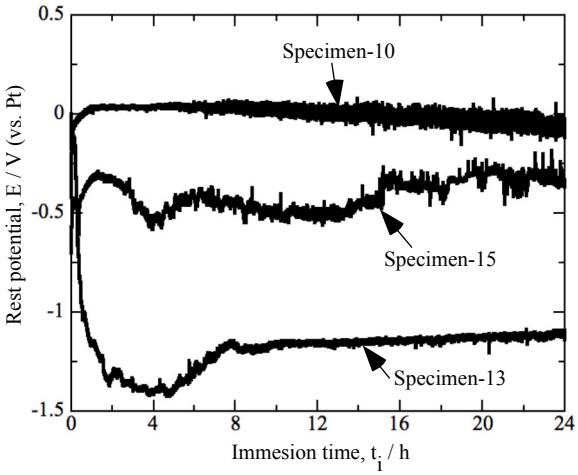
0.5
0
-0.5
-1
-1.5
0
4
8
12
16
20
24
Rest potential, E / V (vs. Pt)
Immesion time, t_i / h
Specimen-10
Specimen-15
Specimen-13

Fig. 6

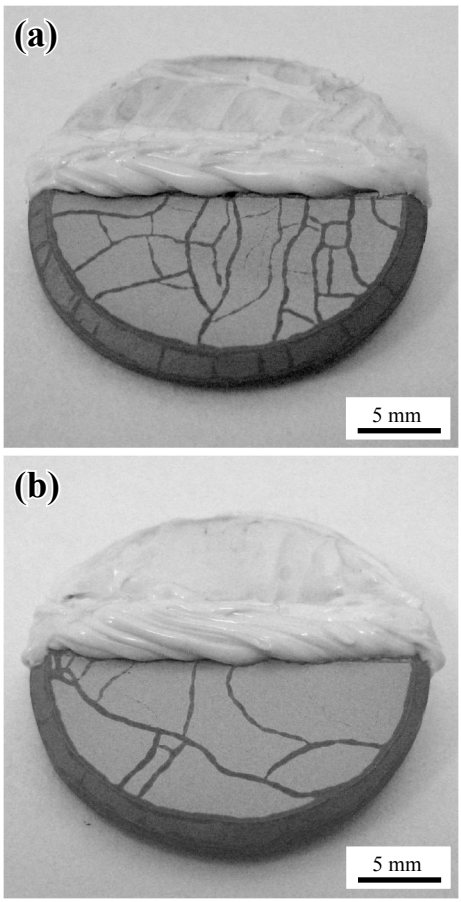

Fig. 7

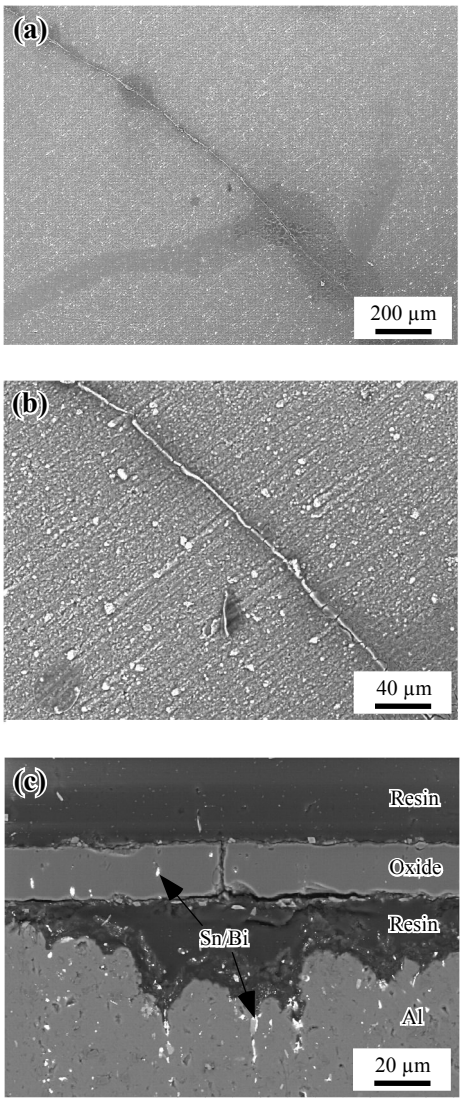

Fig. 8

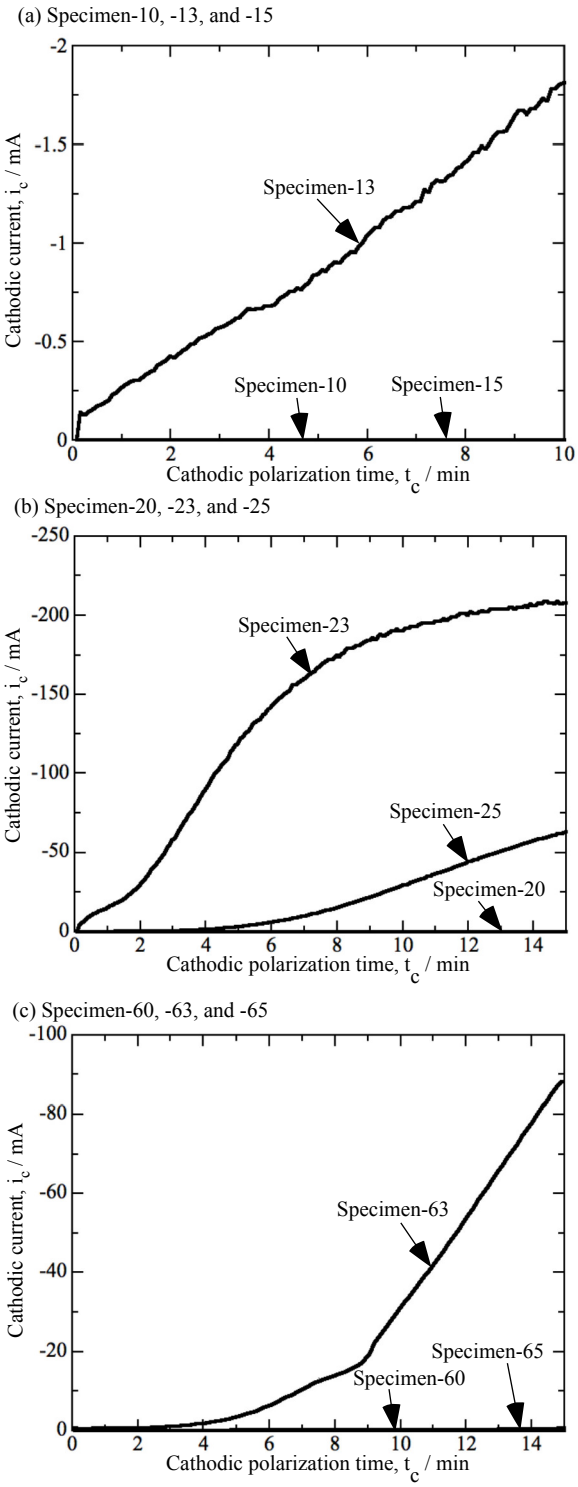
(a) Specimen-10, -13, and -15
Cathodic current, i_c / mA
Cathodic polarization time, t_c / min
Specimen-13
Specimen-10
Specimen-15
(b) Specimen-20, -23, and -25
Specimen-23
Specimen-25
Specimen-20
(c) Specimen-60, -63, and -65
Specimen-63
Specimen-65
Specimen-60

Fig. 9

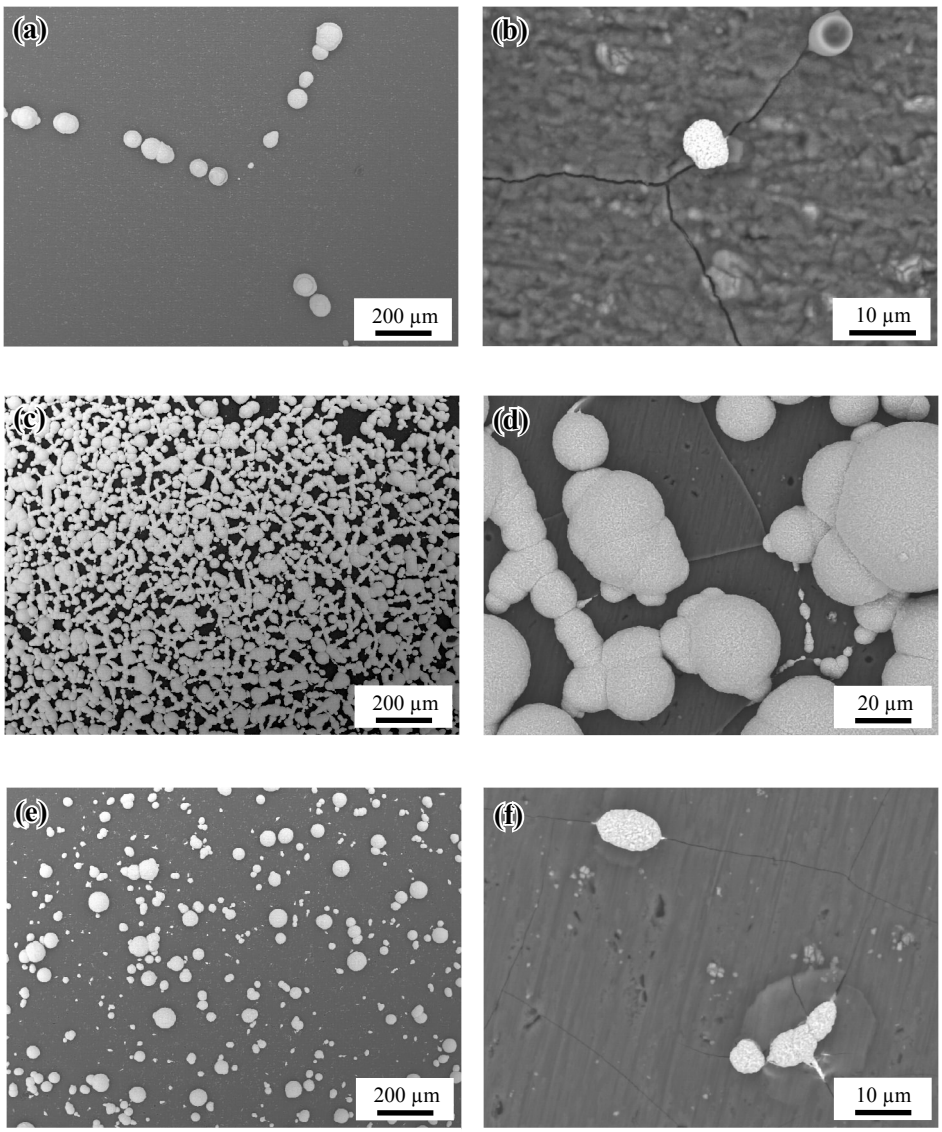

Fig. 10

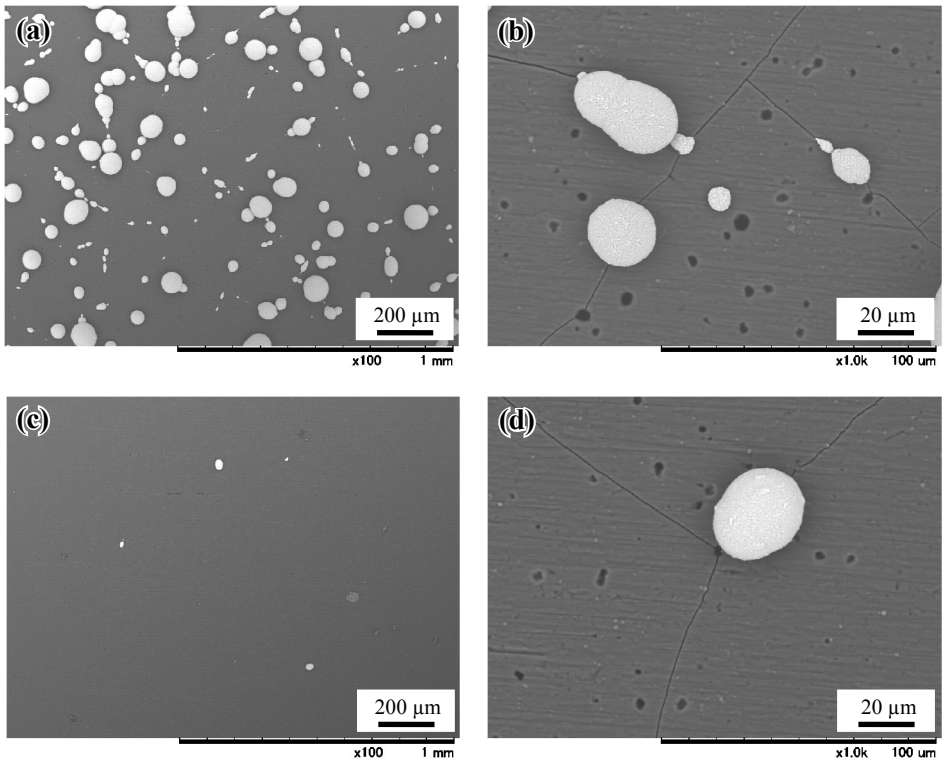
(a)
200 µm
x100 1 mm
(b)
20 µm
x1.0k 100 um
(c)
200 µm
x100 1 mm
(d)
20 µm
x1.0k 100 um

Fig. 11

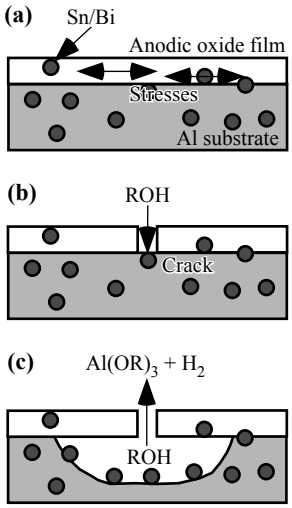
(a)
Sn/Bi
Anodic oxide film
Stresses
Al substrate
(b)
ROH
Crack
(c)
Al(OR)3 + H2
ROH

Fig. 12